Thermodynamic analysis on the fate of ash elements in chemical looping combustion of solid fuels – Manganese-Based oxygen carriers

Fuel 369 (2024) 131676

Contents lists available at ScienceDirect

Fuel

journal homepage: www.elsevier.com/locate/fuel

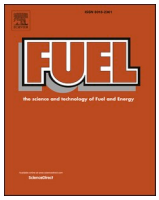

Full Length Article

Thermodynamic analysis on the fate of ash elements in chemical looping combustion of solid fuels – Manganese-Based oxygen carriers

Ivana Staničić [a,*], Joakim Brorsson [b], Anders Hellman [b], Magnus Rydén [a], Tobias Mattisson [a]

[a] Department of Space, Earth and Environment, Division of Energy Technology, Chalmers University of Technology, SE-412 96 Gothenburg, Sweden
[b] Department of Physics, Division of Chemical Physics, Chalmers University of Technology, SE-412 96 Gothenburg, Sweden

ARTICLE INFO

Keywords:
Waste-derived fuels
Ash interaction
Thermodynamic modeling
Phase analysis
First-principles
Chemical looping
Oxygen carriers

ABSTRACT

Chemical looping combustion (CLC) is an innovative technology suitable for converting waste-derived fuels into heat and power. The process inherently produces pure CO_2, which is highly favorable for carbon capture and storage and could be instrumental for achieving negative emissions. CLC operates by utilizing solid oxygen carriers (OCs) to transfer heat and oxygen between two reactors. The OC play a crucial role in achieving an efficient combustion. Manganese-based OCs are particularly interesting, due to their ability to release gaseous oxygen. However, ash components from solid fuels could alter their oxygen transfer capacity, and cause problems related to corrosion and agglomeration. The objective of this work is to obtain in-depth insights about Mn-based OCs for CLC of waste-derived fuels. This is achieved by investigating phase transitions during CLC of solid fuels when utilizing two manganese-based OCs: manganese oxide and a representative manganese ore. For this purpose, thermodynamic modeling is employed, and a specific focus is given to K, Na, Cu, Zn, and Pb, due to their important role in corrosion and/or agglomeration. Thermodynamic databases are expanded by calculating properties from first-principles. It is shown that Mn-based OCs are suitable for effectively converting waste-derived fuels while limiting corrosion. Furthermore, the iron in manganese ores is found to have positive implications for oxygen-transfer reactions. In terms of alkali release to the gas phase, manganese ore seems to be a more promising material compared to manganese oxide. The pathways for the heavy metals Zn, Cu, and Pb were, meanwhile, independent of the OC type.

1. Introduction

To meet the climate targets agreed upon in the Paris Agreement, significant reductions of greenhouse gas emissions are needed along with large-scale removal of CO_2 from the atmosphere. [1] Specifically, this will require neutral and even negative carbon emission technologies. [2] Carbon Capture and Storage (CCS) has been acknowledged as an important strategy for climate mitigation. Even though CCS could be applied to all types of fuels, including fossil fuels, CCS with biomass could have the benefit of generating net-negative emissions. Bio-Energy with Carbon Capture and Storage (BECCS) is an attractive option since it allows for negative emissions while simultaneously producing heat and power. [3,4] Even though biomass removes CO_2 from the atmosphere, via photosynthesis, the same amount is released when it is burned. However, if the released carbon dioxide is captured and stored there will be a net flow out of the atmosphere, i.e., negative emissions.

One technology especially suitable for this purpose is Chemical Looping Combustion (CLC). One major benefit of CLC is that the cost and energy penalties associated with CO_2 capture are among the lowest. [5] The principle of CLC is to use Oxygen Carriers (OCs), in the form of metal oxides, and two interconnected reactors. The OCs transfer heat and oxygen from the Air Reactor (AR) to the Fuel Reactor (FR). The OC is first reduced in the FR by the fuel according to reaction (1) and then oxidized in the AR by air according to reaction (2).

$$(2n + m)Me_xO_y + C_nH_{2m} \rightarrow (2n + m)Me_xO_{y-1} + mH_2O + nCO_2 \quad (1)$$

$$Me_xO_{y-1} + \frac{1}{2}O_2 \rightarrow Me_xO_y \quad (2)$$

Thereafter, the reoxidized OCs are transported back to the FR and the process is repeated. In this way, fuel is converted in a nitrogen-free environment using oxygen from the metal oxides. Consequently, CO_2 is obtained at high concentrations in the FR outlet, which is suitable for CCS. Further, CLC could have some advantages in the case of complex

* Corresponding author.
E-mail address: stanicic@chalmers.se (I. Staničić).

https://doi.org/10.1016/j.fuel.2024.131676
Received 22 December 2023; Received in revised form 22 March 2024; Accepted 8 April 2024
Available online 15 April 2024

fuel compositions. For instance, inorganic ash species are expected to be concentrated in the FR, which is highly advantageous for limiting both emission and corrosion. Since most of the heat-transfer surfaces are in the AR, it is expected that corrosion phenomena should be lower for CLC compared to conventional technologies. This is important because transitioning to renewable energy is expected to result in an expansion of the biomass resource base and the use of waste fuels. [6,7]

The conversion of solid fuels in CLC is complex and involves several steps. First, the fuel is heated in the fluidized bed, and the moisture content is evaporated. The fuel then undergoes devolatilization, removing volatile species. Lastly, the remaining char, mainly C, is gasified by the fluidizing steam or CO_2 according to reactions (3)–(4).

$$C + H_2O \rightarrow CO + H_2 \quad (3)$$

$$C + CO_2 \rightarrow 2CO \quad (4)$$

The volatile end products from the gasification are oxidized by the OC. Char gasification with steam as an oxidizing agent is a relatively slow process at temperatures expected in the fuel reactor, i.e. < 1000 °C, meaning that long residence times and reactor volumes may be needed for complete char conversion. [8] However, there is a way around the slow gasification step. Certain OCs can release gaseous oxygen at relevant conversion temperatures, according to reaction (5). The char can then directly react with gaseous oxygen in reaction (6), meaning that the slow gasification step can be bypassed.

$$2\,Me_xO_y \rightarrow 2\,Me_xO_{y-1} + O_2 \quad (5)$$

$$C + O_2 \rightarrow CO_2 \quad (6)$$

These reaction steps are referred to as Chemical Looping with Oxygen Uncoupling (CLOU). [9] This mechanism avoids the gas–solid reaction between OCs and volatiles. Instead, gaseous oxygen can directly react with the volatiles and facilitate complete conversion, even though the mixing between the OC and fuel is inadequate.

The solid fraction remaining after combustion of a fuel consists of incombustible minerals, known as ash. The ash composition is highly dependent on the type of fuel. Ash can be especially problematic for waste-derived fuels due to elevated concentrations of the metals K, Na, Zn, Cu, and Pb. These elements often combine to form compounds, mainly in the form of metal chlorides, that can cause corrosion and fouling. Furthermore, gaseous chlorides can also promote reactions with silicates, which could cause agglomeration due to the low melting point of alkali silicates. Interestingly, when OCs are used in combustion processes, they can serve as a sink for some ash elements. This has positive implications, as it can mitigate issues related to corrosion and agglomeration.

CLC is a breakthrough technology for carbon capture, and it has been demonstrated for over 11,000 h in more than 50 pilot units. [10] Only limited work has concerned biomass and waste-derived fuels. Instead, most work has focused on fossil fuels. While Mn-based OCs have been studied, there is currently no knowledge on how they perform with waste-derived fuels. The main objective of this study is to answer this question.

1.1. Oxygen carriers with CLOU properties

There are several OCs with CLOU properties, including copper and manganese oxides. Although both are interesting, the disadvantage of copper is the high cost along with the low melting temperature while manganese displays slow kinetics of reoxidation at low temperatures. Rydén et al. [11] showed that the thermodynamic properties of manganese oxides can be altered through combination with other metals such as iron, silicon, calcium, nickel, magnesium, and copper. Azimi et al. [12] tested combinations of Mn–Fe–O, Mn–Si–O as well as Mn–Fe–Si and all showed promising results. There are several studies conducted on the performance of different manganese-based OCs [13,14] but the literature regarding ash interactions is scarce. In fact, only a few combined ash-OC phases have been reported for these oxide systems. [15–17] Mineral ores are especially interesting OCs due to their low cost and high reactivity. Besides manganese oxide, these also contain other components such as Fe, Ca, Si and Mg. While manganese containing minerals are distributed across all continents of the world [18], their elemental composition can vary substantially [19,20]. Since Mn ores are still abundant and relatively cheap, they could be highly applicable for CLC, especially with solid fuels.

Single perovskites have the general formula $ABO_{3-\delta}$ where A and B are different cations. The oxygen deficiency varies depending on the temperature and surrounding oxygen partial pressure. With decreasing O_2 partial pressure, oxygen is released from the structure, resulting in a higher δ-value. This is taken advantage of during CLC, as the perovskite will be oxidized in the AR and release oxygen in the FR. Manganese-based perovskites, such as $CaMnO_{3-\delta}$, in which Mn has been substituted with other transition metals, have been examined extensively as OCs and is of interest for both CLC and CLOU. [21,22] Several perovskite-type OCs have been studied with solid fuels in 10 kW [23,24] and 100 kW [25] CLC units.

1.2. Role of thermodynamic modeling

Multiphase multicomponent equilibrium calculations have been applied to obtain a better understanding of the chemical transformations during thermochemical conversion of fuels, and also for predicting ash-related problems during fuel conversion. Such calculations are used to determine stable chemical and physical forms in a system, as function of parameters such as temperatures, pressures, and the elemental composition of input streams. By minimizing Gibbs free energy under an elemental balance constraint, stable solid and gaseous phases can be monitored, given that thermodynamic data for all possible phases and compounds is available. [26] It is not uncommon to combine experimental tests with thermodynamic predictions as done by Hildor et al. [27]. A recent study by Staničić et al. [28] investigated the fate of several ash components in CLC of biomass and waste using two iron-based oxygen carriers with help of the software FactSage 8.1™ [29] and associated databases. The incorporation of first-principles thermodynamic data of identified crystalline phases contributed to the most comprehensive and updated thermodynamic study of these important systems to date.

1.3. Aim of study

The main objective of this study is to investigate whether Mn-based materials are applicable for CLC of waste-derived fuels. This study explores the phase transitions occurring in CLC of solid fuels utilizing manganese-based OCs. Given the scarcity of prior research in the field, this paper carries the novelty of reporting the expected phase transitions occurring in CLC of solid fuels, and also the consequences of implementing solid fuels with Mn-based OCs. The effect on OC performance and possible regeneration is addressed together with correlations with available literature. A deeper understanding is achieved by using multiphase multicomponent thermodynamic equilibrium calculations to monitor phases in the FR and AR while simultaneously studying the effect of different fuels, ash contents in the bed, and two Mn-based OCs, i.e., Mn-oxide and Mn-ore. These were chosen as the results with Mn-oxide gives specific information about Mn-interactions, while manganese ore is more realistic with respect to use as an OC since it contains significant fractions of other elements. FactSage™ 8.2 is employed along with the databases FactPS, FToxid, FTsalt and HSCA. The selected elements in focus are Cl, K, Na, S, Zn, Cu, and Pb. The influence of the OCs on the solid phase distribution and elements is also considered together with implications on CLC operation and possible remedies. In particular, this study involved the following four steps: i) a comprehensive and

detailed review of existing literature concerning manganese-based OCs, ii) assessment of identified phases from the literature and correlations with existing thermodynamic databases, iii) incorporation of results from first-principles calculations of thermodynamic properties for selected compounds, for which no thermodynamic data is available in the literature, e.g. $CaMnO_{3-\delta}$ and iv) implementation of expanded databases to study manganese-based systems and correlations between simulations and experimental observations.

2. Method

The CLC reactors were modeled in the software FactSage™ 8.2 [29] using the databases FactPS, FToxid, FTsalt and HSCA. Specifically, FactPS contains data for pure substances, FToxid data for pure oxides; oxide solid solutions as well as molten solutions, and FTsalt data for pure salts together with salt solutions. HSCA contains data for pure substances, which are not found in any of the aforementioned databases. The data was collected from HSC Chemistry 9 and 10 [30] and has been used in previous work.[31,32] A complete list of phases and abbreviations is provided in Table S 3 in the Supplementary Information (SI).

Two manganese-based OCs, in the form of Mn-oxide and a representative Mn-ore, are investigated along with two fuels, specifically branches and treetops (BT) as well as recycled waste wood (RWW). The OC and ash compositions are presented in Table 1 and Table 2 respectively. Data for the two fuels were obtained from [33] and they have been used in previous work by Staničić et al. [28]. The fuels were chosen to represent different compositions found in both natural and waste-derived biomass. Notably, RWW contains higher levels of inorganic elements, particularly heavy metals, as observed in Table 2. Furthermore, since the compositions of Mn-ore can vary widely depending on the origin, mean values were calculated from 19 different ores reported by Sundqvist et al. [19,20] and used in this study. The corresponding averages and standard deviations for Mn-ore is presented in Table 1.

The solids circulation rate, an important parameter in CLC, is determined by performing a heat balance given the requirement that the transport of sensible heat from the AR to the FR is sufficient for a temperature of 950℃ to be maintained in the latter. Also, the reducing potential of the atmosphere in the FR is set to $\log_{10}(p_{O_2}) = -13.2$atm, see Staničić et al. [28] for further details. According to the model, the FR is adiabatic and fluidized with CO_2 preheated to 400℃, while the AR is fluidized with air preheated to 400℃. Also, the oxygen concentration in the exhaust gas is 5 %. It is, furthermore, assumed that the OC entering the FR is fully oxidized with a temperature of 1050℃, that the oxygen-carrying phases in the Mn-ore are the major constituents Mn_3O_4 and Fe_2O_3, as well as that the temperature and reduction levels are homogenous in both reactors.

Accumulation of ash requires special attention in CLC of solid fuels. It is expected that lighter ash particles will follow the FR exhaust gas and that the ash will be separated from the OC before entering the AR. For example, ash particles could be separated by a cyclone since they have a lower density than the OCs. Nevertheless, some ash may remain in the system, especially when using fuels with high ash contents. Another transportation path could be by interaction with the OC or the formation of sticky compounds on the OC surface. Therefore, the fate of ash components in the AR will also be discussed in this paper. More specifically, it is assumed that all solid ash particles in the FR will be transferred to the AR. Though this is a worst-case scenario, it is useful for illustrating the importance of effective ash separation. The maximum amount of ash investigated is around 65–70 wt% of the total fluidized bed, which is an extreme case that will likely not be achieved with biomass fuels. Waste fuels, on the other hand, contain significantly larger ash fractions compared to biomass. By investigating high ash fractions in the bed, it is expected that a better picture of the possible transformations, in the form of either ash-OC or ash-ash-based reactions, is obtained. The ash concentration in the bed is calculated as the difference between the total mass of the solid phases and the total reduced OC in the FR (the monoxide MnO) or oxidized OC in the AR (Mn_2O_3, Mn_3O_4 named *Te-SPINA*, Mn_7SiO_4, and $CaMn_2O_4$) divided by the total mass of the solids. The ash concentration is represented by a white dashed line in the diagrams. Phase formation with increasing ash concentrations will be presented for each fuel and OC to illustrate the effect of ash components while the release of elements will be discussed based on the initial calculation, with the lowest ash concentration.

Table 1
Composition of two manganese-based oxygen carriers used in this study. The standard deviations indicated for manganese ore are based on an analysis of compositions of different ores, obtained from Sundqvist et al. [19], (2017).

[wt%]	Mn-oxide	Mn-ore
Mn_3O_4	100	56.1 ± 19.6
Fe_2O_3		20.5 ± 17.9
SiO_2		7.6 ± 4.5
CaO		5.6 ± 5.8
Al_2O_3		2.9 ± 3.6
K_2O		0.7 ± 0.4
MgO		1.8 ± 1.9
Na_2O		0.3 ± 0.2
P_2O_5		0.1 ± 0.1
TiO_2		0.2 ± 0.3

Table 2
Composition of ashes from branches and treetops (BT) and recycled waste wood (RWW) obtained from [33].

Ash composition [wt%]	Branches and treetops	Recycled Waste Wood
Ca	19.2	6.8
Si	11.3	11.6
Al	2.0	2.7
Fe	0.8	2.3
Ti	0.1	1.8
Mn	1.6	0.2
Mg	2.1	1.2
Na	0.9	1.4
K	7.6	2.1
P	1.7	0.18
Ba	0.27	0.33
Cu	0.011	0.059
Pb	0.007	0.054
Zn	0.2	1.04

2.1. First-principles calculations

The utilization of first-principles to obtain thermodynamic data has been implemented in the first part of this study [28] and details on the method have been published separately. [34] In short, this involved computing reaction energies using density functional theory, as well as the phononic contribution to the heat capacity under the harmonic approximation. In accordance with the procedure presented by Benisek and Dachs [35], the results from these ab initio calculations were combined with experimental data from the NIST-JANAF thermochemical tables to determine the enthalpy and entropy at room temperature together with the temperature dependence of the heat capacity. For reference, the same approach has previously been shown to yield excellent agreement with experimental data when applied to $FeTiO_3$. [28,34] The discrepancy between the calculated and experimental data for $FeTiO_3$ is below 2.8 J/molK, 0.89 kJ/mol, and 2.0 J/molK for the heat capacity, formation enthalpy, and entropy, respectively. The procedure is further described in section 1 of the SI. This approach was utilized for species identified experimentally in relevant CLC experiments, but where data was lacking in the abovementioned standard databases. The influence of these compounds on the thermodynamic calculations will be discussed in detail.

Manganese-based perovskites, where Mn is partially replaced by other transition metals, have been examined extensively as OCs. [36]

The lack of thermodynamic data for systems other than stoichiometric $CaMnO_3$, and in particular oxygen-deficient perovskites, could lead to significant discrepancies between experiments and calculations. To address this issue, a semi-empirical model originally proposed by Goldyreva et al. [37] was used to calculate the difference in heat capacity, formation enthalpy and entropy of $CaMnO_{3-\delta}$ relative to $CaMnO_3$. This information was, in turn, combined with the data for the stoichiometric phase found in the FToxid database, to obtain estimates of the same properties for 31 discrete δ-values in steps of $\delta = 1/64$, which are listed in Table S2. The procedure is described in detail in Section 2 of the SI.

3. Results and discussion

A summary of crystalline phases reported for manganese-based OCs used in chemical looping applications, which have all been identified in laboratory-scale experiments, is presented in Table 3. Most of the reported ash-induced crystalline phases in Mn-based materials stem from one publication, [16]where FactSage 7.2 was utilized. It is worth noting that the databases have since been updated, especially with respect to the Mn-system. Mn_2O_3 has, for example, been optimized on several binary and ternary subsystems and added to the $CaO\text{-}MgO\text{-}Al_2O_3\text{-}SiO_2\text{-}FeO\text{-}Fe_2O_3\text{-}MnO$ system. In FactSage 7.3, 18 new stoichiometric compounds, amongst these Mn_7SiO_{12}, were added to the database. More importantly, the slag and spinel phases now includes the Mn^{3+} component, which is significant in this study. However, there is still experimental data missing for several relevant compounds and these were obtained in two ways, as explained in more detail below.

Table 3
Identified crystalline phases of combined ash and manganese-based oxygen carriers used in chemical looping applications. All studies are performed in laboratory scale units. Compounds that are not available in thermodynamic databases are presented in bold. Synthesized oxygen carriers are presented in quotation with the main metal components.

Oxygen carrier	Ash compound	Phases reported in the literature		Ref
		Oxidizing	Reducing	
Mn_3O_4	K_2CO_3 $CaCO_3$	**$KMnO_4$**	**K_2MnO4** (Ca,Mn)O	[15]
6 % SiO_2 + Mn_3O_4	K_2CO_3 $Ca_3(PO_4)_2$	**K_2MnO4**	**$K_2Mn_2O_3$** **$Ca_{19}Mn_2(PO_4)_{14}$**	[15]
10 % SiO_2 + Mn_3O_4	K_2CO_3 $Ca_3(PO_4)_2$	**K_2MnO_4**	**$K_2Mn_2O_3$** Ca_2SiO_4 **$Ca_{19}Mn_2(PO_4)_{14}$**	[15]
25 % SiO_2 + Mn_3O_4	$Ca_3(PO_4)_2$	$Ca_3(PO_4)_2$	**$Ca_{19}Mn_2(PO_4)_{14}$**	[15]
Hausmannite	$CaCO_3$ K_2CO_3 SiO_2	$CaMn_2O_4$ **$CaMnO_3$** **K_2MnO_4** **K_3MnO_4**	**$K_2Mn_4O_8$** **$CaMn_7O_{12}$**	[17]
"MnSi"	$CaCO_3$	$CaSiO_3$ **$CaMn_{14}SiO_{24}$**	**$CaMn_{14}SiO_{24}$**	[16]
	K_2CO_3	**$K_2Si_4O_9$** **K_2MnO_4** **$K_{1.03}Mn_2O_4$**	**$K_2Si_4O_9$** **K_2MnO_4**	
	$CaHPO_4$	**$Ca_{19}Mn_2(PO_4)_{14}$**	**$Ca_{19}Mn_2(PO_4)_{14}$** **$CaSiO_3$**	
"MnSiTi"	$CaCO_3$	$CaTiO_3$ **$CaSiO_3$**	**$CaMn_{14}SiO_{24}$**	[16]
	K_2CO_3	**$K_2Ti_4O_9$** **K_4SiO_9** **K_2MnO_4**	**$K_2Ti_2O_5$** **K_2SiO_3** **K_2MnO_4** **$K_2TiSi_6O_{15}$**	
	$CaHPO_4$	**$Ca_{19}Mn_2(PO_4)_{14}$** **$CaMnTi_2O_6$**	**$Ca_{19}Mn_2(PO_4)_{14}$**	
"MnFe"	$CaCO_3$	$CaFe_2O_4$	$Ca_2Mn_{0.2}Fe_{1.8}O_5$ (Ca,Mn)O $Ca_2Fe_2O_5$	[16]
	K_2CO_3	**$KFeO_2$** **K_2FeO_4** **K_2MnO_4**	**$KFeO_2$**	
	$CaHPO_4$	**$Ca_9Fe(PO_4)_7$** **$Ca_{19}Mn_2(PO_4)_{14}$**	**$Ca_{9.33}Fe_{1.167}(PO_4)_7$** **$Ca_{19}Mn_2(PO_4)_{14}$** (Fe,Mn,Ca)O	
"MnFeAl"	$CaCO_3$	$Ca_2Fe_2O_5$ **$Ca_{0.55}Al_{11}O_{17.05}$**	$Ca_2Fe_2O_5$ **$Ca_2Al_{1.38}Fe_{0.62}O_5$**	[16]
	K_2CO_3	**$KFeO_2$** **$KAlO_2$** **K_2FeO_4** **K_2MnO_4**	**$KFeO_2$** **$KAlO_2$**	
	$CaHPO_4$	**$Ca_9Al(PO_4)_7$** **$Ca_{19}Mn_2(PO_4)_{14}$**	**$Ca_9Fe(PO_4)_7$** **$Ca_9Al(PO_4)_7$** **$Ca_{19}Mn_2(PO_4)_{14}$**	

3.1. Thermodynamic data from First-Principles

A comparison between phases reported in the literature and FactSage databases FactPS and FToxid revealed the following inconsistencies: $Ca_{19}Mn_2(PO_4)_{14}$, $CaMn_{14}SiO_{24}$, K_2MnO_4, K_3MnO_4, KMn_2O_4, and $CaMnO_{3-\delta}$. Thermal properties for these compounds, with an exception for $CaMnO_{3-\delta}$, were calculated from first-principles, and are listed in Table S1 in the SI. As is shown by Brorsson et al. [34], the first principles data have an impact on the K–Mn–O system. For example, KMn_2O_4, K_2MnO_4, and K_3MnO_4 are all stable at 950 °C and 1 atm given that the partial oxygen pressure is sufficiently high ($p_{O_2} \gtrsim 10^{-11}$ atm). As should be expected, KMn_2O_4 dominates at a low K/Mn ratio ($K/(K+Mn) \lesssim 0.35$). K_3MnO_4 also begins to form for a close to equal content of K and Mn. The other phases, $Ca_{19}Mn_2(PO_4)_{14}$ and $CaMn_{14}SiO_{24}$, are not found to be stable under reasonable CLC conditions. More details are provided in the literature [34].

3.2. Thermodynamic data for $CaMnO_{3-\delta}$

Though the stoichiometric compound $CaMnO_3$ is available in FactPS, this phase is known to release and capture oxygen at different reduction degrees, which is not accounted for in the solution phases. In this study, 31 compounds with varying δ-values were therefore added to the database to represent $CaMnO_{3-\delta}$. Specifically, these were generated by adding corrections, calculated via a semi-empirical model for δ between 0 and 0.5 in steps of $\delta = 1/64$, to the thermodynamic data for stoichiometric $CaMnO_3$. The influence of these calculated compounds in the Ca-Mn-O phase diagram is plotted in red and presented in Fig. 1. The operating conditions and the range of temperatures and oxygen partial pressures where the perovskite phase is stable can be seen in the figure. Under oxidizing conditions, the perovskite $CaMnO_3$ is stable up to 809 °C. Different temperatures and reduction degrees are required for the decomposition of the perovskite. A summary of possible decomposition reactions and conditions based on the calculated data is presented in Table 4. The reversible reduction from $CaMnO_3$ to $CaMn_2O_4$ and $Ca_2MnO_{4-\delta}$ has been observed experimentally at 1000 °C by Bakken et al. [38] which is consistent with the new data in Table 4 and Fig. 1.

Previous studies of $CaMnO_{3-\delta}$ have determined the oxygen content, given by 3-δ, experimentally for different temperatures in air. Specifically, Bakken et al. [38] report the oxygen content to be 2.929 ± 0.003, 2.902 ± 0.002, and 2.878 ± 0.005 at 950 °C, 1000 °C, and 1050 °C, respectively. On the other hand, Rørmark et al. [39] report oxygen contents of 2.956 and 2.93 at 950 °C and 1000 °C, respectively. The results thus deviate significantly, which could be due to the differences in the experimental approach as reasoned by Bakken et al. [38]. In this study, the thermodynamic limit for the oxygen content at 950 °C, 1000 °C, and 1050 °C is 2.96875, 2.953125 and 2.921875 in pure O_2, and 2.953125, 2.921875, 2.90625 in air. These results agree better with the values reported by Rørmark et al. [39]. However, it is important to note that the choice of reference data influences the outcome. Here, thermal data for the stoichiometric solid $CaMnO_3$ from FToxid was utilized as it has been optimized with respect to other relevant Ca-Mn-phases in the system.

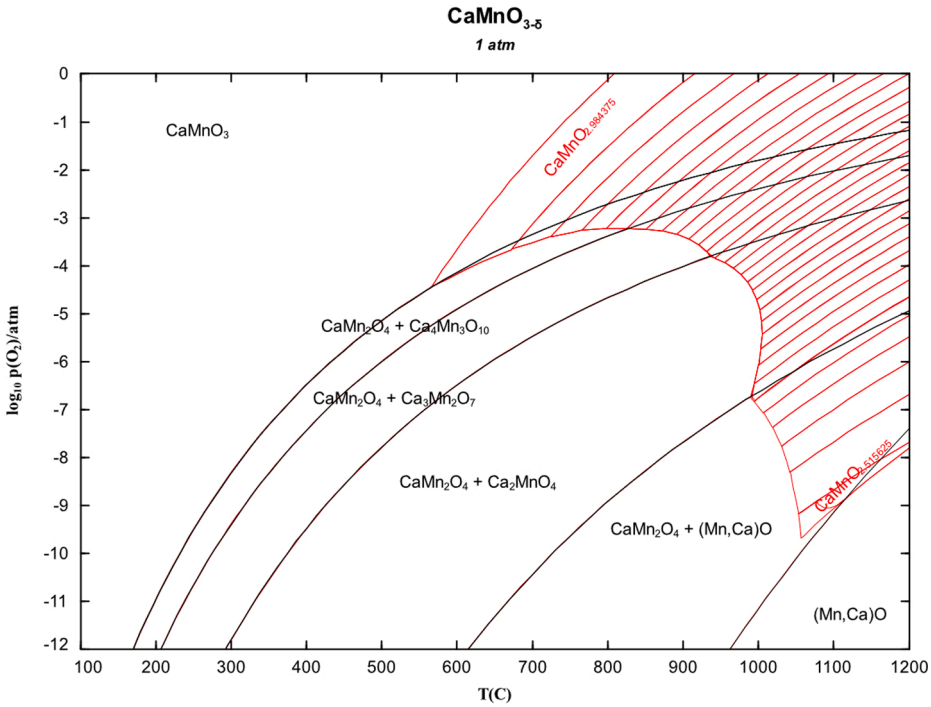

Fig. 1. Stable phases in the perovskite system, $CaMnO_{3-\delta}$, at 1 atm showing $\log_{10}(pO_2)$ versus temperature before and after (red) implementation of the calculated data. The phase transitions in red represent reductions (from left to right) in (3-δ) in steps of 1/64. (For interpretation of the references to colour in this figure legend, the reader is referred to the web version of this article.)

Table 4
Summary of possible decomposition reactions of the perovskite $CaMnO_{3-\delta}$ according to thermodynamic data obtained from first-principles presented in Fig. 1. The temperature (T) interval in °C and oxygen partial pressure (p_{O_2}) in atm are presented in the table.

Thermodynamic Prediction of Decomposition Reactions	Conditions
$CaMnO_{3-\delta} \rightarrow \frac{1}{5}CaMn_2O_4 + \frac{1}{5}Ca_4Mn_3O_{10} + \frac{1}{10}O_2$	$565 < T < 825$ $10^{-4.5} < p_{O_2} < 10^{-3.2}$
$CaMnO_{3-\delta} \rightarrow \frac{1}{4}CaMn_2O_4 + \frac{1}{4}Ca_3Mn_2O_7 + \frac{1}{8}O_2$	$825 < T < 937$ $10^{-3.8} < p_{O_2} < 10^{-3.2}$
$CaMnO_{3-\delta} \rightarrow \frac{1}{3}CaMn_2O_4 + \frac{1}{3}Ca_2MnO_4 + \frac{1}{6}O_2$	$937 < T < 1004$ $10^{-6.7} < p_{O_2} < 10^{-3.8}$
$CaMnO_{3-\delta} \rightarrow \frac{1}{2}CaMn_2O_4 + \frac{1}{2}CaO + \frac{1}{4}O_2$	$990 < T < 1056$ $10^{-9.7} < p_{O_2} < 10^{-6.7}$
$CaMnO_{3-\delta} \rightarrow CaO + MnO + \frac{1}{2}O_2$	$T > 1056$ $p_{O_2} > 10^{-9.7}$

3.3. Chemical looping combustion using manganese oxide

The major phase distribution in the FR and AR with increasing ash content when using Mn-oxide is presented in Fig. 2 for BT (Fig. 2a-b) and RWW (Fig. 2c-d). While the amount of ash increases along the x-axis, the actual level is represented by the dashed white line and is shown on the secondary y-axis. Regardless of the fuel, the main phase in the FR is monoxide ((Mn,Ca)O), which has also been observed experimentally, see Table 3. Olivine ($(Ca,Mn)_2SiO_4$)), $KAlSiO_4$ and $K_2Ca_2Si_4O_{15}$ increase with the ash content in the FR when using BT. The slag is also included here, and its main components are K_2O, CaO, SiO_2, P_2O_5, and MnO. In the AR, the most stable phases are tetragonal spinel (*Te-SPINA* - $(Mn,Al,Mg,Fe,Zn)_3O_4$), $CaMn_2O_4$, leucite (*Leu* - $K_2Al_2Si_4O_{12}$), and olivine (*OlivA* - $(Ca,Mg,Fe,Mn,Zn)_2SiO_4$). Here, the slag composition is slightly different and includes more SiO_2 as well as some K_2O, CaO, P_2O_5 and MgO.

Comparable results are obtained for RWW, but in this case nepheline ($(Na,K)AlSiO_4$) and $CaTiO_3$ are observed in the FR instead of $KAlSiO_4$ and $K_2Ca_2Si_4O_{15}$, respectively. In this case, the slag consists of SiO_2, MnO, $NaAlO_2$, CaO, $KAlO_2$, and Na_2O. These discrepancies can be explained by the fact that RWW contains less Ca but the same amount of Si, which has implications for the chemistry. More substantial differences are found in the AR. Specifically, there is a tendency for Mn to form Mn_7SiO_{12} instead of $CaMn_2O_4$, especially at an intermediate ash content. In addition, olivine (*OlivA* - $(Mn,Ca,Mg,Fe,Zn)_2SiO_4$) is more abundant than leucite (*Leu* - $K_2Al_2Si_4O_{12}$), which is also partially replaced by first $CaTiO_3$ and then $CaSiTiO_5$. The slag in the AR, meanwhile, consists of SiO_2, MnO, $NaAlO_2$, $KAlO_2$, and CaO. These observations show that the fuel composition (see Table 2), affects the chemistry not only in the FR but also the AR.

The influence of ash on the stability of OC phases can be followed in Fig. 2. Though the oxygen transfer reaction occurs mainly between Mn_3O_4 and MnO, it is affected by the ash. Specifically, olivine (*OlivA* - $(Mn,Ca,Mg,Fe,Zn)_2SiO_4$) become stable in the FR with increasing ash content. Still, at the highest ash concentration, 86 % and 64 % of the total Mn remain in the monoxide phase for BT and RWW, respectively. In the AR there is a combination of the spinel (Te-SPINA, Mn_3O_4), $CaMn_2O_4$, and Mn_7SiO_{12} (only for RWW), the latter two of which form because Ca and Si are introduced by the ash. At the highest ash level, about 16 % of the total Mn is bound as $CaMn_2O_4$ and 58 % as Mn_3O_4, while the maximum Mn_7SiO_{12} content is 20 %. Hence, it is clear that the main oxygen transfer reactions occur via the main oxide system, even at higher ash concentrations. Since Rydén et al. [11] has shown that the phase Mn_7SiO_{12} is a viable CLOU material, it should be an active OC here as well. If the perovskite $CaMnO_{3-\delta}$ is used as an OC, it is generally undesirable to have a transition to $CaMn_2O_4$ [40] but this phase could still transform and release oxygen in the FR in monoxide systems as predicted here.

3.4. Chemical looping combustion using manganese ore

Fig. 3 shows the major phase distribution in the FR and AR with increasing ash content for BT (Fig. 3a-b) and RWW (Fig. 3c-d) when using Mn-ore. As in Fig. 2, the amount of ash increases along the x-axis

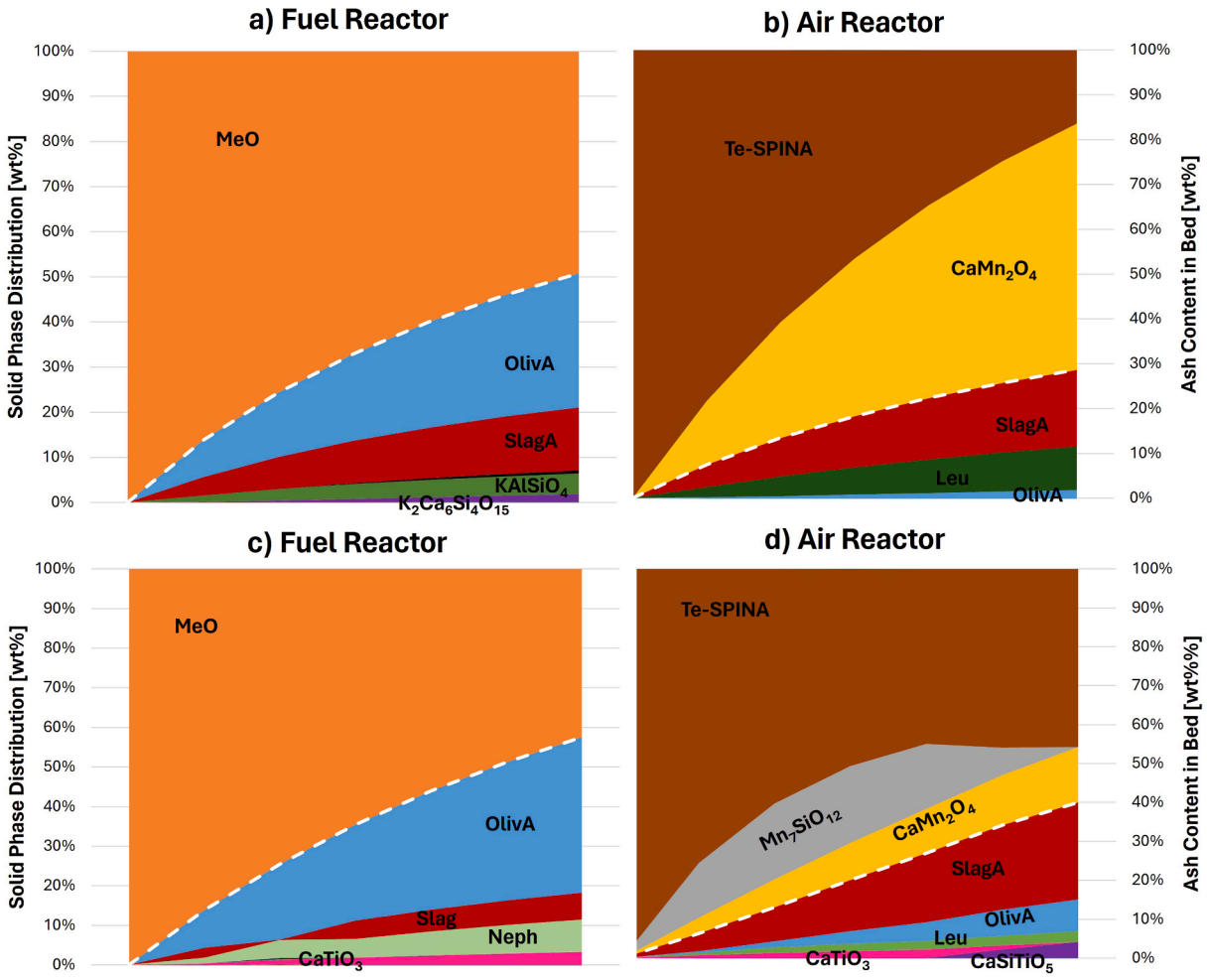

Fig. 2. Solid phase distribution during CLC utilizing Mn-oxides as the oxygen carrier. FR operates at 1 atm and 950°C for BT (a) and RWW (c). AR operates at 1 atm and 1050°C for BT (b) and RWW (d). The ash content in the bed is presented in the secondary y-axis. The ash concentration is represented by a white dashed line in the diagrams.

and the actual level is represented by the dashed white line, which corresponds to the secondary y-axis. According to Fig. 3, the phase distribution more or less follows the same trends when Mn-ore serves as the OC instead of Mn-oxide, although a few additional phases can be observed in the FR. Due to other elements present in the ore, olivine (*OlivA* - $(Mn,Ca,Mg,Fe,Zn)_2SiO_4$), nepheline (*Neph* - $(K,Na)(Al,Fe)SiO_4$) and $Na_2Ca_3Al_{16}O_{28}$ are, for example, present in the bed from the start. Another difference is that the slag is less stable in the FR for both fuels, which is due to the inherent high fraction of Ca in the ore. Also, the composition changes from MnS, FeS, MnO, FeO, SiO_2, and CaS at the lowest ash concentrations to K_2O, CaO, P_2O_5, SiO_2 and MnO at higher. In the AR, Mn_7SiO_{12} is not stable for RWW, which is likely due to the concentration of Ca in the Mn-ore. For both fuels, an additional phase appears, namely clinopyroxene ($CaMgSi_2O_6$)), at the lowest, and in the case of BT also the highest, ash levels. At the same time, both slag and olivine ($(Mn,Ca,Mg,Fe,Zn)_2SiO_4$) are more abundant in the AR, especially at low ash contents.

More significant changes are observed in the AR, of which the most dramatic is the formation of a significant amount of $(Fe,Mn)_2O_3$ (*M_2O_3*) at the cost of a major reduction of tetragonal spinel (*Te-SPINA* Mn_3O_4). This is due to the high concentrations of iron in the Mn-ore, which allows oxidation to not only $(Fe,Mn)_3O_4$ but also $(Fe,Mn)_2O_3$. This will have positive implications for the oxygen transport as the material can be further oxidized and reduced compared to the case with Mn-oxide, and also have CLOU properties. One of the main drivers for the use of Mn-ores has been the possibilities to inherently obtain combined Mn-oxides with these types of properties. In the AR there is a combination of the $(Fe,Mn)_3O_4$, $(Fe,Mn)_2O_3$, and $CaMn_2O_4$ along with smaller amounts of olivine and slag. For both fuels, most Fe is found as $(Fe,Mn)_2O_3$. With increasing ash contents, there are similarities between the fuels because less Mn is bound to the spinel $(Fe,Mn)_3O_4$ and more is associated with $(Fe,Mn)_2O_3$ and $CaMn_2O_4$. At the highest ash concentration 13 % and 4 % of the total Mn is found in the slag as MnO for RWW and BT, respectively. Similar to the case with Mn-oxide, the higher amount of slag can be attributed to the lower amount of Ca, but the same amount of Si, in RWW.

The influence of ash on the stability of OC phases can be followed in Fig. 3. The oxygen transfer reaction occurs mainly from (Fe,Mn)O to $(Fe,Mn)_3O_4$ and $(Fe,Mn)_2O_3$, the latter of which forms due to the high contents of iron in the ore. In the FR, 87 % of the total Mn is found as MnO and 13 % in olivine, as Mn_2SiO_4 and partly $CaMnSiO_4$, for both fuels. At the highest ash concentration, 87 % and 66 % of the total Mn remain in the monoxide phase for BT and RWW, respectively. The rest forms olivine, with an increasing fraction of $CaMnSiO_4$.

3.5. *Fate of ash components*

The ash components Cl, S, K, Na, Zn, Cu and Pb are of particular importance for the chemical processes occurring within the reactors. To provide a more detailed view of the pathways of inorganic elements in the CLC process, Sankey-diagrams are provided in Fig. 5 for branches and treetops, with Mn-oxide and Mn-ore as OCs. Similar illustration for

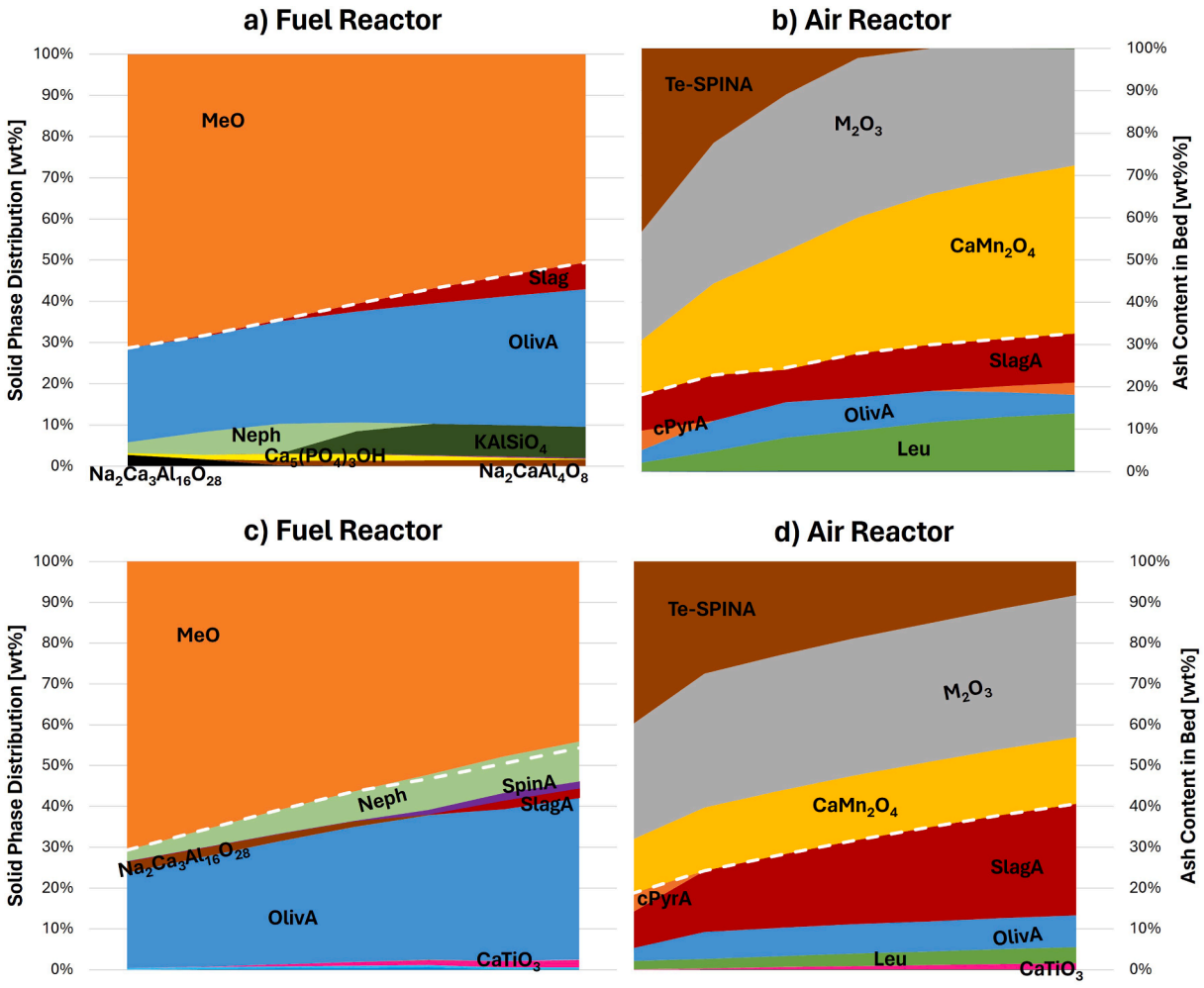

Fig. 3. Solid phase distribution during CLC utilizing Mn-ore as the oxygen carrier. FR operates at 1 atm and 950°C for BT (a) and RWW (c). AR operates at 1 atm and 1050°C for BT (b) and RWW (d). The ash content in the bed is presented in the secondary y-axis. The ash concentration is represented by a white dashed line in the diagrams.

recycled waste wood (Figure S 3) can be found in the SI. These figures illustrate the proportion of inorganic elements released into the gas phase within the fuel and air reactors, as well as the resulting solids in the latter. Specifically, the diagrams show the distribution of the fuel components S, Cl, Na, K Cu, Pb and Zn, which have been normalized in a way that maintains the same weight ratio between the elements as in the fuel. Furthermore, it is assumed that all solids from the fuel reactor are transferred to the air reactor, as described in Section 2.

Since the selection of OC can be vital to minimizing the adverse effects of the ash, it is interesting to compare the results from the study at hand with data obtained from comparable calculations for Fe-based OCs by Staničić et al. [28]. A summary of the distribution between the gaseous and solids phases is presented in Table 5 for the different combinations of fuels (BT and RWW) and both Mn- and Fe-based OCs. Since BT contains a lower amount of S, Cl, and ash compared to RWW the total mass released can be higher for RWW, even at conditions where the entire content is released to the gas phase for BT. This is illustrated by the colors, where green corresponds to the highest mass released, red is the lowest and clear cells represent values in between. It is evident from Table 5 (and through comparative analysis of Fig. 5 and Figure S3 in SI) that CLC of RWW yields the highest concentration of inorganic species within the gaseous phase in the FR. According to Table 5, which includes previously published data for iron oxide and iron–titanium oxide (ilmenite), there are substantial differences in terms of the amounts of the most problematic ash elements that are released into the gas phase depending on the fuel and OC. For example, the table shows that CLC of RWW using Mn-ore as an OC will result in the least amount of alkali metals and heavy metals released to the gas phase, closely followed by ilmenite. On the other hand, Mn-oxide has the highest release, followed by Fe-oxide. Furthermore, it is found that all chloride-bearing compounds, which include HCl, KCl, NaCl, and $PbCl_2$, will be concentrated in the FR outlet. Thus, the worst corrosion-related issues are expected in the FR independent of the type of OC. Zinc also shows a clear difference in behavior depending on the OC. For the Mn-based, Zn is found in the monoxide (MeO) phase as (Zn, Mn, Fe)O, while for Fe-oxide it is bound in the spinel (SPINA) as $ZnFe_2O_4$. The release to the gas phase is, thus, low in all cases except for ilmenite for which a large share enters the gas phase since all iron is bound in ilmenite or titania spinel ($FeTiO_3$ or $FeTi_2O_4$) and these solid solutions do not dissolve Zn. Copper, on the other hand, is generally expected to remain in the solid phase, while lead is released to the gas phase independent of the OC type.

A summary of the phases in the AR and FR, and the influence of the ash concentration on several essential elements is given below for the Mn-based OCs. The elements Cl, K, Na, S, Pb, Cu, and Zn are in focus because of their important role in melt formation and corrosion. A separate discussion for Fe-based OCs can be found in literature [28]. The raw data showing the phase distribution for each investigated element is included in the appended Excel sheet.

Chlorine. Cl enters the gas phase in the FR primarily as KCl and some

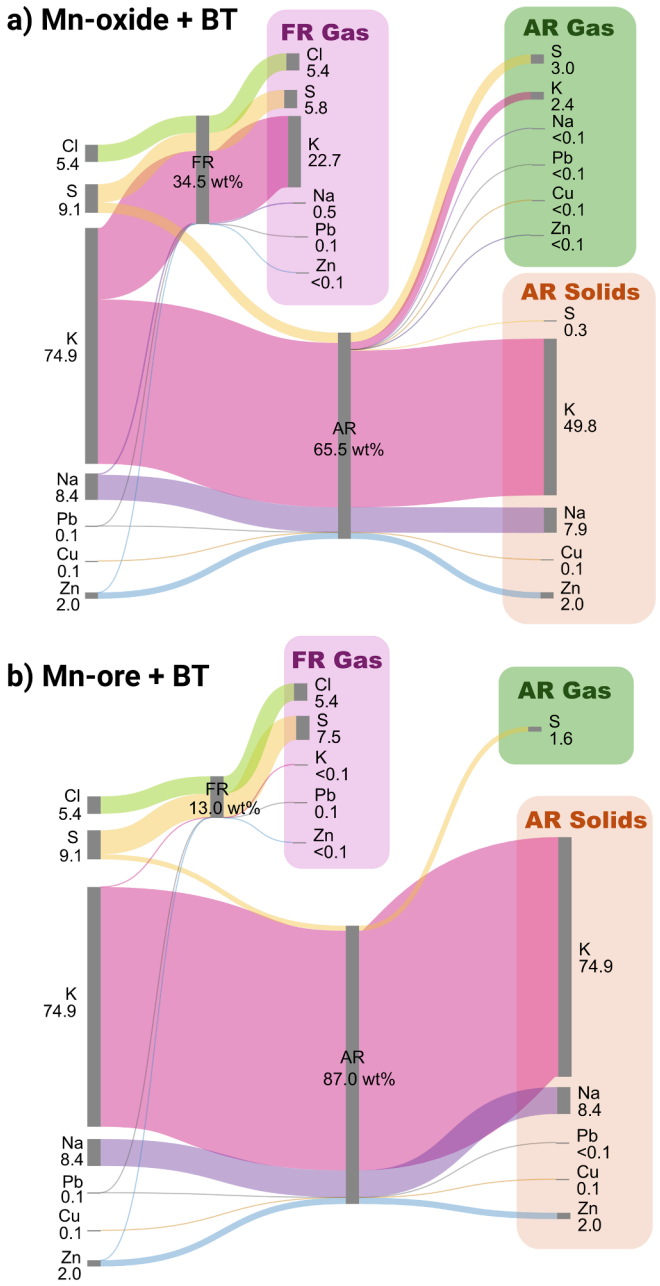

Fig. 5. Sankey-diagrams illustrating the distribution of selected elements (Cl, S, Na, K, Pb, Cu and Zn) in the fuel and air reactors during chemical looping combustion (CLC) of branches and treetops (BT) as fuel. Two oxygen carriers, a) manganese oxide and b) manganese ore, are compared. The elements are normalized but retain the same weight ratio as in the fuel.

HCl. The amount of NaCl is always lower than KCl. This indicates that the most corrosive compounds will be concentrated in the FR outlet, thus leaving the AR free from chloride compounds. This is true for both Mn-based OCs as shown in Fig. 5 and Figure S3 in SI.

Sulfur. The primary reason for the difference in the gas phase release for the Mn-based OCs is the solid phase MnS, which only forms for Mn-oxide. For the ore, S is retained in the slag with the main components FeS and MnS. As can be seen from Table 5 and Fig. 5, a significant amount leaves with the gas in the form of H_2S and PbS, for both Mn-based OCs. For Mn-oxide, the proportion of gaseous compounds drops to less than 20 % as the ash content increases, and for Mn-ore even faster.

The situation is drastically different in the AR where most S is found as SO_2 for both oxygen carriers and all fuels at the lowest ash content. For BT, and increasing ash contents, K_2SO_4 (*alpha-K2SO4*) dominates at all ash fractions, except for the lowest. For RWW, different trends are observed. For Mn-oxide the major solid phase is $(Na,K)_2SO_4$ (*Salt-liquid*), which only forms at a low to intermediate, but not the lowest, ash content. For Mn-ore all S that is carried over to the AR from the FR, leaves with the gas, primarily as SO_2.

Potassium. There are clear differences in the gas phase release for the two Mn-based OCs as observed in Fig. 5. For Mn-oxide, KOH and KCl are the two major gas components in the FR, while K_3PO_4 and K_2O (in the slag) is the principle solid phase when using BT. Nepheline ($(K,Na)(Al,Fe)SiO_4$) and $K_2Ca_6Si_4O_{15}$ both increase with the ash concentration; in the case of RWW the former dominates over K_2O except at the very lowest ash level. In contrast to Mn-oxide, no K is released from the FR for Mn-ore (Fig. 5). Instead, it primarily forms nepheline ($(K,Na)(Al,Fe)SiO_4$) together with a certain amount of K_2O and $KAlO_2$, in the slag. For RWW, the concentrations of the latter two slag components are almost negligible except at high ash contents, but in the case of BT the proportion of K found as K_2O reaches as high as 40 %.

In the AR, for Mn-oxide, most K forms K_2SO_4, of which some is released as a gas, while the rest remains in the slag or as leucite ($K_2Al_2Si_4O_{12}$). For Mn-ore, however, no gaseous K compounds form, and instead, leucite and slag represent the main phases.

Sodium. Some similarities with K concerning the gaseous release can be observed. In the FR, a small amount leaves with the gas phase as NaOH, and in the case of RWW also NaCl. With BT as fuel, the rest is mostly kept in the slag as Na_2O, although the amount of $Na_2CaAl_4O_8$, and to a lesser extent nepheline ($(K,Na)(Al,Fe)SiO_4$), increase with the ash content. For Mn-ore, the same phases are observed although at different proportions; $Na_2CaAl_4O_8$ is followed by Na_2O and $Na(Al,Fe)O_2$ (in the slag) and finally nepheline ($(K,Na)(Al,Fe)SiO_4$). For RWW, nepheline and the slag components Na_2O and $NaAlO_2$ are stable for both OCs. In the AR, less than 1 % is released as gaseous Na or Na_2SO_4, while the primary form remains to be Na_2O in the slag for Mn-oxide, but also $Na(Al,Fe)O_2$ for Mn-ore. In other words, almost no gaseous Na compounds form in any of the reactors as observed in Fig. 5.

Lead. The situation in the FR is more or less the same for both OCs, as illustrated in Fig. 5. Over 99 % of the total Pb leaves the FR as PbS (g) and Pb (g), but this fraction drops below 40 % as the ash content increases. The remaining part consists of PbO, which is absorbed by the slag phase and carried over to the AR, where it is partially released as PbO (g). In particular, the gaseous proportion decreases from about 99.9 % to 3.9 % as the amount of ash increases. For Mn-ore, no gaseous compounds are formed in the AR; instead Pb is fully dissolved in the slag as PbO.

Copper. Copper is primarily found in the solids for all investigated cases, as shown in Fig. 5 and Figure S3 in the SI. For Mn-oxide, when using BT, Cu is found in the slag as Cu_2O in the FR, except at the lowest ash level where the monoxide CuO dominates. While the latter observation also applies to RWW, most of the Cu_2O is replaced by Cu_3As. By contrast, Cu_2O forms almost exclusively in the AR for both fuels. These observations also apply to the Mn-ore with a few minor differences. More precisely, the only compound that forms in the FR when using BT is Cu_2O. In the case of RWW, meanwhile, Cu_3As is the main phase even though it coexists with a certain amount of Cu_2O and CuO. Together, the latter two contain up to 60 % of the Cu, but this proportion drops to below 6 % as the ash content increases.

Zinc. For Mn-oxide and both fuels, Zn is encountered in the monoxide phase as ZnO, but for a higher ash content, Zn becomes associated with olivine (*OlivA* - $(Mn,Ca,Mg,Fe,Zn)_2SiO_4$). When these are carried over to the AR, olivine becomes the most stable phase followed by slag, while the monoxide is completely absent. In the case of Mn-ore and BT, the same compounds are observed in the FR, in similar proportions. For RWW, on the other hand, tetragonal spinel (*Te-SPINA*, $(Mn,Al,Mg,Fe,Zn)_3O_4$), also forms at high ash contents, which eventually becomes more abundant than olivine. The situation in the AR is reversed, as the slag is the main phase, followed by olivine for both fuels.

Table 5
The weight percent of elements released to the gas phase in the FR, at the lowest ash concentration, for BT and RWW and the oxygen carriers Mn-oxide and Mn-ore. Data for the oxygen carriers ilmenite and Fe-oxide presented in the table origin from a previous study by Staničić et al. [28]. The release is illustrated by the colors, where green corresponds to the highest mass released and red the lowest while clear cells represent values in between.

Release to the gas phase [wt% of the total amount]	BT				RWW			
Oxygen Carrier	Mn-oxide	Mn-ore	Fe-oxide	Ilmenite	Mn-oxide	Mn-ore	Fe-oxide	Ilmenite
S	64.1	82.7	99.98	99.97	41.2	52.7	62.3	96.7
Cl	100	100	100	100	100	100	100	100
K	30.3	0.01	13.1	0.9	78.9	0.03	11.7	6.8
Na	5.4	0.0	2.1	0.4	7.7	0.00	1.9	4.4
Zn	0.04	0.02	0.1	98.9	0.03	0.02	0.03	29.7
Cu	0.04	0.0	0.6	0.5	0.04	0.00	0.1	0.00
Pb	99.9	96.1	100	99.99	99.9	88.1	99.96	99.3

3.6. Insights into Mn-based OCs

Understanding the stability of Mn-based OCs is crucial for effective utilization in CLC. The insights gained in this study show that Mn-based OCs can resist deactivation induced by ash. As observed in Figs. 2 and 3, the oxygen transfer reactions occur mainly between Mn_3O_4 and MnO. Even at the highest ash concentrations in the bed, a significant amount of Mn remains in an oxygen-carrying phase. While ashes from waste-derived fuels introduce phases that are inert with respect to oxygen-carrying capability, they can also contribute to new OC phases. For example, the two major ash components Ca and Si promote the formation of the two OC phases $CaMn_2O_4$ and Mn_7SiO_{12}. This makes Mn-based OCs suitable for CLC of waste-derived fuels since the main oxygen transfer reactions occur via the main oxide system, even at high ash concentrations. This shows that Mn-based OCs contribute to effective fuel conversion in the FR, where a pure CO_2 stream is produced suitable for CCS.

As can be gathered from the results for both Mn-based OCs, none of the compounds, for which thermodynamic properties were generated via first-principles calculations, are predicted to form in any appreciable amounts. However, there are subsystems where the K-Mn-O phases are stable. In this study, the system is more complex, and the K-concentration significantly differs from the experiments where these compounds were obtained (see Table 3). In addition, one should keep in mind that the calculations are based on several assumptions. Kinetics are, for instance, not considered and the resulting predictions will, hence, not include any metastable materials. So, the stability of K-Mn-O compounds in real applications should not be overlooked. Ash components can, for example, stick to the OC surface, creating conditions favorable for these phases.

For the non-stoichiometric compound $CaMnO_{3-\delta}$, it is worth noting that the relative stabilities of the phases are highly dependent on the choice of reference data when $\delta = 0$. In particular, the corrections obtained for $\delta > 0$, when applying the defect model described in Section 2 of the SI, were added to the thermodynamic properties for $CaMnO_3$ available in the FToxid database. As a result, the operating conditions in the FR fall outside the range of temperatures and partial oxygen pressures where $CaMnO_{3-\delta}$ is stable, as can be seen from Fig. 1. This does, however, not explain the absence of the perovskite in the AR where the conditions are favorable, according to Fig. 1. Studying the phase transitions under oxidizing conditions, it was found that the ash, specifically SiO_2, prohibits the formation of the perovskite. This is because combined Mn-Si phases, such as olivine $(Ca,Mn)_2SiO_4$ and braunite Mn_7SiO_{12}, are more stable; see the phase diagrams for the AR (Fig. 2b, d and 3b,d). Based on these observations, it is debatable whether perovskites ($CaMnO_{3-\delta}$) have an advantage over other Mn-bearing OCs, such as Mn-oxides and Mn-ores, for CLC of solid fuels because the perovskite could lose its active phase due to the interaction with the ash components. This should be closely considered before implementing perovskites in CLC of solid fuels, and especially waste-derived fuels with high ash contents. Perovskite systems where Mn-sites are substituted with other transition metals could potentially resist such decomposition. This prospect was, however, not possible to investigate in this paper due to limitations in available thermodynamic data. Even so, it should be noted that such perovskite OCs have been successfully employed with gaseous fuels. [41–43] While this study has expanded thermodynamic databases for manganese-based systems and provided valuable insights, there still exists limited thermodynamic data for perovskite systems where the Mn-sites have been substituted with other transition metals.

4. Conclusions

This work shows that manganese-based oxides are highly interesting for CLC of waste-derived fuels. Specifically, a key advantage is that corrosive compounds will leave with the gas in the fuel reactor. This is beneficial because problems related to corrosion and fouling are completely avoided in and downstream of the air reactor, where the majority of heat-transfer surfaces are located. Furthermore, CO_2 is obtained in pure form from the FR, meaning that CLC can be integrated with CCS and is thereby suitable for achieving negative emissions. This study shows that Mn-ore and Mn-oxides are suitable materials for effectively converting waste-derived fuels by CLC. The functionality of the oxygen carrier is expected to be maintained during operation, even with high ash fractions in the CLC system. Although new phases form, such as $CaMn_2O_4$ and Mn_7SiO_{12}, these evidently have a propensity to transfer oxygen from air to fuel. Thus, Mn-based oxygen carriers show resilience against deactivation when utilized in CLC of waste-derived fuels. The iron content in manganese ore has positive implications for oxygen transfer reactions as it allows for oxidation to $(Fe,Mn)_2O_3$, in contrast to manganese oxide which only oxidizes to Mn_3O_4. Considering the release of alkali in the FR there are clear differences between the OCs. The highest alkali release is expected with Mn-oxide since the impurities in Mn-ore can act as sinks for alkali metals. The fates of Zn, Cu, and Pb on the other hand, are largely independent of the OC type. Zn and Cu are expected to stay in the solid phase while Pb devolatilize completely and is released to the gas phase in the fuel reactor. Additionally, due to the propensity to form slag under oxidizing conditions at higher temperatures, this paper also illustrates the importance of ash separation due to higher risks of agglomeration in the AR. Implementing the new thermodynamic data for the oxygen deficient perovskite $CaMnO_{3-\delta}$ showed that certain ash species, specifically SiO_2, decrease the stability of the perovskite due to the formation of combined Mn-Si-phases. This indicates that the perovskite could lose its active phase due to interaction with ash components. Thus, it is debatable whether the perovskite $CaMnO_{3-\delta}$ has an advantage over other Mn-bearing OCs, such as Mn-ore for CLC of solid fuels.

CRediT authorship contribution statement

Ivana Staničić: Writing – original draft, Software, Investigation, Formal analysis. **Joakim Brorsson:** Writing – review & editing, Writing – original draft, Software, Methodology. **Anders Hellman:** Writing – review & editing, Supervision, Methodology. **Magnus Rydén:** Writing – review & editing, Supervision. **Tobias Mattisson:** Writing – review & editing, Supervision, Methodology, Conceptualization.

Declaration of competing interest

The authors declare that they have no known competing financial interests or personal relationships that could have appeared to influence the work reported in this paper.

Data availability

Data will be made available on request.

Acknowledgement

This work was financed by the Swedish Research Council (2016-06023 and 2020-03487). The first-principles calculations were enabled by resources provided by the National Academic Infrastructure for Supercomputing in Sweden (NAISS) and the Swedish National Infrastructure for Computing (SNIC) at C3SE (Göteborg) and NSC (Linköping) partially funded by the Swedish Research Council through grant agreements no. 2022-06725 and no. 2018-05973.

Appendix A. Supplementary data

Supplementary data to this article can be found online at https://doi.org/10.1016/j.fuel.2024.131676.

References

[1] Gasser T, Guivarch C, Tachiiri K, Jones CD, Ciais P. Negative emissions physically needed to keep global warming below 2 °C. Nat Commun 2015;6:7958.
[2] Azar C, Lindgren K, Obersteiner M, Riahi K, van Vuuren DP, den Elzen KMGJ, et al. The feasibility of low CO2 concentration targets and the role of bio-energy with carbon capture and storage (BECCS). Clim Change 2010;100:195–202.
[3] Fajardy M, Morris J, Gurgel A, Herzog H, Mac Dowell N, Paltsev S. The economics of bioenergy with carbon capture and storage (BECCS) deployment in a 1.5 °C or 2 °C world. Glob Environ Change 2021;68:102262.
[4] Kemper J. Biomass and carbon dioxide capture and storage: A review. Int J Greenh Gas Control 2015;40:401–30.
[5] Abanades JC, Arias B, Lyngfelt A, Mattisson T, Wiley DE, Li H, et al. Emerging CO2 capture systems. Int J Greenh Gas Control 2015;40:126–66.
[6] Bogner J, Pipatti R, Hashimoto S, Diaz C, Mareckova K, Diaz L, et al. Mitigation of global greenhouse gas emissions from waste: conclusions and strategies from the Intergovernmental Panel on Climate Change (IPCC) Fourth Assessment Report. Working Group III (Mitigation). Waste Manag Res ISWA 2008;26:11–32.
[7] IPCC, 2014. Climate Change 2014: Synthesis Report. Contribution of Working Groups I, II and III to the Fifth Assessment Report of the Intergovernmental Panel on Climate Change in: Pachauri, R., Meyer, L. (Eds.).
[8] Leion H, Mattisson T, Lyngfelt A. The use of petroleum coke as fuel in chemical-looping combustion. Fuel 2007;86:1947–58.
[9] Mattisson T, Lyngfelt A, Leion H. Chemical-looping with oxygen uncoupling for combustion of solid fuels. Int J Greenh Gas Control 2009;3:11–9.
[10] Di Giuliano A, Capone S, Anatone M, Gallucci K. Chemical looping combustion and gasification: A review and a focus on european research projects. Ind Eng Chem Res 2022;61:14403–32.
[11] Rydén M, Leion H, Mattisson T, Lyngfelt A. Combined oxides as oxygen-carrier material for chemical-looping with oxygen uncoupling. Appl Energy 2013;113:1924–32.
[12] Azimi G, Leion H, Rydén M, Mattisson T, Lyngfelt A. Investigation of different Mn-Fe oxides as oxygen carrier for chemical-looping with oxygen uncoupling (CLOU). Energy Fuels 2013;27:367–77.
[13] Andersson V, Soleimanisalim AH, Kong X, Leion H, Mattisson T, Pettersson JBC. Alkali interactions with a calcium manganite oxygen carrier used in chemical looping combustion. Fuel Process Technol 2022;227:107099.
[14] Mei D, Lyngfelt A, Leion H, Mattisson T. Study of the interaction between a Mn ore and alkali chlorides in chemical looping combustion. Fuel 2023;344:128090.
[15] Leion H, Knutsson P, Steenari BM. Experimental evaluation of interactions between K, Ca and P and Mn/Si-based oxygen carriers, european biomass conference and exhibition proceedings. ETA-Florence Renewable Energies 2017:660–5.
[16] Staničić I, Andersson V, Hanning M, Mattisson T, Backman R, Leion H. Combined manganese oxides as oxygen carriers for biomass combustion — Ash interactions. Chem Eng Res Des 2019;149:104–20.
[17] Staničić I, Hanning M, Deniz R, Mattisson T, Backman R, Leion H. Interaction of oxygen carriers with common biomass ash components. Fuel Process Technol 2020;200:106313.
[18] Cannon, W.F., Kimball, B.E., Corathers, L.A., 2017. Manganese, in: Schulz, K.J., DeYoung, J.J.H., Seal Ii, R.R., Bradley, D.C. (Eds.), Professional Paper, Reston, VA, p. 40.
[19] Sundqvist S, Arjmand M, Mattisson T, Rydén M, Lyngfelt A. Screening of different manganese ores for chemical-looping combustion (CLC) and chemical-looping with oxygen uncoupling (CLOU). Int J Greenh Gas Control 2015;43:179–88.
[20] Sundqvist S, Khalilian N, Leion H, Mattisson T, Lyngfelt A. Manganese ores as oxygen carriers for chemical-looping combustion (CLC) and chemical-looping with oxygen uncoupling (CLOU). J Environ Chem Eng 2017;5:2552–63.
[21] Ahmad A, Al Mamun MA, Al-Mamun M, Huque S, Ismail M. LFO perovskites as oxygen carriers for chemical looping oxygen uncoupling (CLOU). J Therm Anal Calorim 2022;147:6605–13.
[22] Wang X, Gao Y, Krzystowczyk E, Iftikhar S, Dou J, Cai R, et al. High-throughput oxygen chemical potential engineering of perovskite oxides for chemical looping applications. Energy Environ Sci 2022;15:1512–28.
[23] Schmitz M, Linderholm C, Lyngfelt A. Chemical Looping combustion of sulphurous solid fuels using spray-dried calcium manganate particles as oxygen carrier. In: Dixon T, Twinning S, Herzog H, editors. 12th international conference on greenhouse gas control technologies, GHGT 2014. Austin, USA: Elsevier Ltd; 2014. p. 140–52.
[24] Schmitz M, Linderholm CJ. Performance of calcium manganate as oxygen carrier in chemical looping combustion of biochar in a 10 kW pilot. Appl Energy 2016;169:729–37.
[25] Gogolev I, Linderholm C, Gall D, Schmitz M, Mattisson T, Pettersson JBC, et al. Chemical-looping combustion in a 100 kW unit using a mixture of synthetic and natural oxygen carriers – Operational results and fate of biomass fuel alkali. Int J Greenh Gas Control 2019;88:371–82.
[26] Lindberg D, Backman R, Chartrand P, Hupa M. Towards a comprehensive thermodynamic database for ash-forming elements in biomass and waste combustion — Current situation and future developments. Fuel Process Technol 2011;105:129–41.

[27] Hildor F, Zevenhoven M, Brink A, Hupa L, Leion H. Understanding the interaction of potassium salts with an ilmenite oxygen carrier under dry and wet conditions. ACS Omega 2020:22966–77.
[28] Staničić I, Brorsson J, Hellman A, Mattisson T, Backman R. Thermodynamic analysis on the fate of ash elements in chemical looping combustion of solid fuels—iron-based oxygen carriers. Energy Fuels 2022;36:9648–59.
[29] Bale CW, Bélisle E, Chartrand P, Decterov SA, Eriksson G, Gheribi AE, et al. FactSage thermochemical software and databases - 2010–2016. Calphad 2016;54:35–53.
[30] Roine., A., 2018. HSC Chemistry® [Software], Outotec, Pori.
[31] Staničić I, Backman R, Cao Y, Rydén M, Aronsson J, Mattisson T. Fate of trace elements in Oxygen Carrier Aided Combustion (OCAC) of municipal solid waste. Fuel 2021;122551.
[32] Staničić I, Mattisson T, Backman R, Cao Y, Rydén M. Oxygen carrier aided combustion (OCAC) of two waste fuels - Experimental and theoretical study of the interaction between ilmenite and zinc, copper and lead. Biomass Bioenergy 2021;148:106060.
[33] Strömberg B, Herstad Svärd S. Bränslehandboken 2012 [The Fuel Handbook 2012]. VÄRMEFORSK ISSN 2012:1653.
[34] Brorsson J, Staničić I, Gastaldi J, Mattison T, Hellman A. Thermodynamic properties for metal oxides from first-principles. Comput Mater Sci 2024;233:112690.
[35] Benisek A, Dachs E. The accuracy of standard enthalpies and entropies for phases of petrological interest derived from density-functional calculations. Contrib Mineral Petrol 2018;173:90.
[36] Rydén M, Lyngfelt A, Mattisson T, Chen D, Holmen A, Bjørgum E. Novel oxygen-carrier materials for chemical-looping combustion and chemical-looping reforming; LaxSr1-xFeyCo1-yO3-δ perovskites and mixed-metal oxides of NiO, Fe2O3 and Mn3O4. Int J Greenh Gas Control 2008;2:21–36.
[37] Goldyreva EI, Leonidov IA, Patrakeev MV, Kozhevnikov VL. Thermodynamics of oxygen in CaMnO3 − δ. J Solid State Electrochem 2013;17:3185–90.
[38] Bakken E, Norby T, Stølen S. Nonstoichiometry and reductive decomposition of CaMnO3−δ. Solid State Ion 2005;176:217–23.
[39] Rørmark L, Wiik K, Stølen S, Grande T. Oxygen stoichiometry and structural properties of La1 - xAxMnO3 ± δ (A = Ca or Sr and 0 ≤ x ≤ 1). J Mater Chem 2002;12:1058–67.
[40] Hallberg P, Jing D, Rydén M, Mattisson T, Lyngfelt A. Chemical looping combustion and chemical looping with oxygen uncoupling experiments in a batch reactor using spray-dried CaMn1−xMxO3−δ (M = Ti, Fe, Mg) particles as oxygen carriers. Energy Fuels 2013;27:1473–81.
[41] Hallberg P, Källén M, Jing D, Snijkers F, Van Noyen J, Rydén M, et al. Experimental investigation of CaMnO3-δ based oxygen carriers used in continuous chemical-looping combustion. Int J Chem Eng 2014:2014.
[42] Källén M, Rydén M, Dueso C, Mattisson T, Lyngfelt A. CaMn0.9Mg0.1O3-δ as oxygen carrier in a gas-fired 10 kWthchemical-looping combustion unit. Ind Eng Chem Res 2013;52:6923–32.
[43] Rydén M, Lyngfelt A, Mattisson T. CaMn0.875Ti0.125O3 as oxygen carrier for chemical-looping combustion with oxygen uncoupling (CLOU)—Experiments in a continuously operating fluidized-bed reactor system. Int J Greenh Gas Control 2011;5:356–66.